

Modeling the genetic and mechanical interplay in osteoarthritis: from in vitro systems to mechanistic insights Bloks. N.G.C.

Citation

Bloks, N. G. C. (2025, October 22). *Modeling the genetic and mechanical interplay in osteoarthritis: from in vitro systems to mechanistic insights*. Retrieved from https://hdl.handle.net/1887/4279635

Version: Publisher's Version

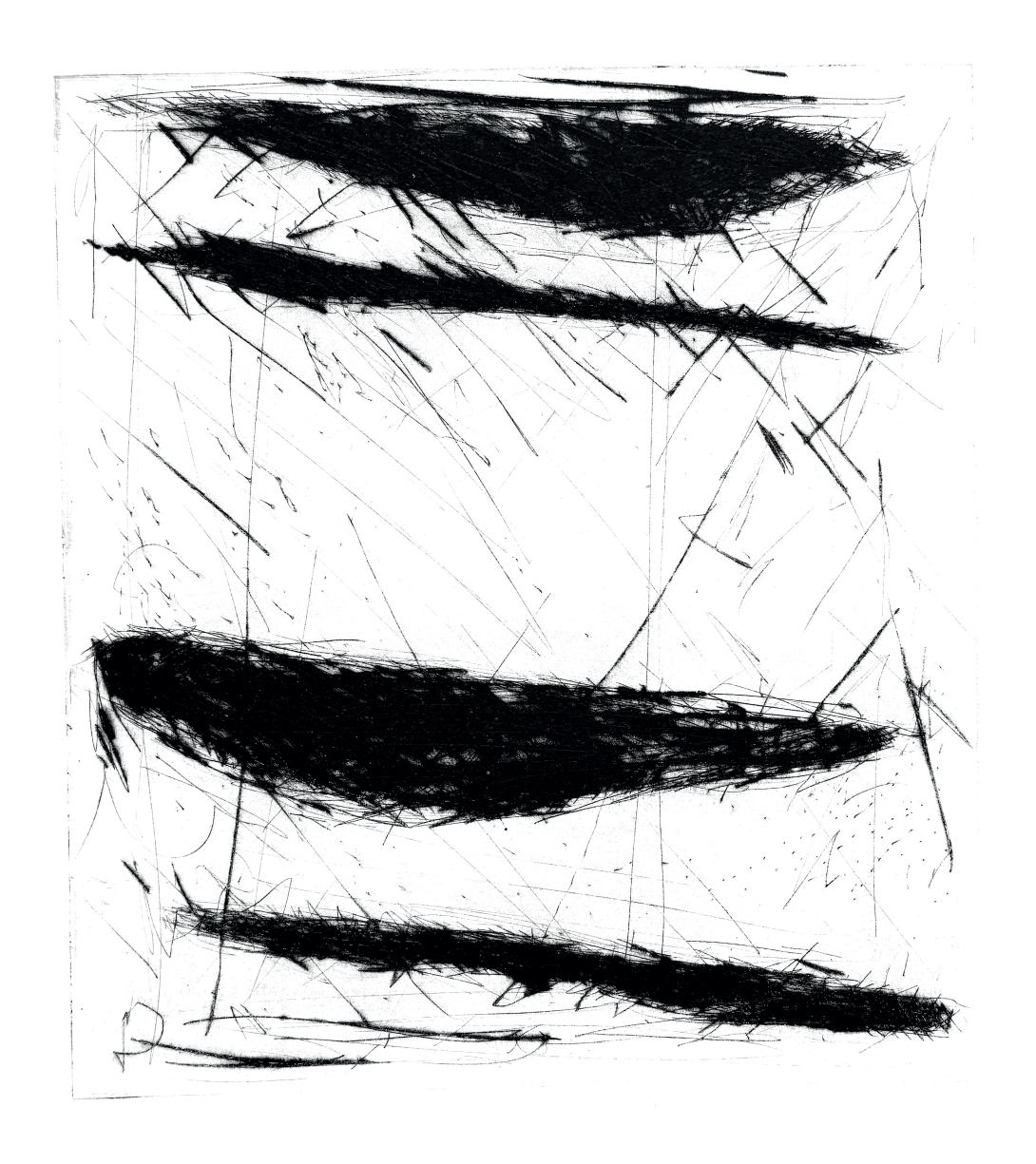
Licence agreement concerning inclusion of doctoral

License: thesis in the Institutional Repository of the University

of Leiden

Downloaded from: https://hdl.handle.net/1887/4279635

Note: To cite this publication please use the final published version (if applicable).



PETER M.G COX 1988

CHAPTER 4

Hyper-physiologic mechanical cues, as an osteoarthritis disease relevant environmental perturbation, cause a critical shift in set-points of methylation at transcriptionally active CpG sites in neo-cartilage organoids

Niek GC Bloks^{1, *}, Amanda Dicks^{2,3,*}, Zainab Harissa^{2,3}, Rob GHH Nelissen⁴, Ghazaleh Hajmousa¹, Yolande FM Ramos¹, Rodrigo Coutinho de Almeida¹, Farshid Guilak^{2,3,†}, Ingrid Meulenbelt^{1,†}

¹Dept. Biomedical Data Sciences, Section Molecular Epidemiology, Leiden University Medical Center,
Leiden, The Netherlands

²Washington University, Saint Louis, MO, USA

³Shriners Hospitals for Children, Saint Louis, MO, USA

⁴Department of Orthopedics, Leiden University Medical Center, Leiden, The Netherlands.

*Shared first author †Shared last author

Abstract

Background

Osteoarthritis (OA) is a complex, age-related multifactorial degenerative disease of diarthrodial joints marked by impaired mobility, joint stiffness, pain, and a significant decrease in quality of life. Among other risk factors, such as genetics and age, hyperphysiological mechanical cues are known to play a critical role in the onset and progression of the disease (1). It has been shown that post-mitotic cells, such as articular chondrocytes, heavily rely on methylation at CpG sites to adapt to environmental cues and maintain phenotypic plasticity. However, these long-lasting adaptations may eventually have a negative impact on cellular performance. We hypothesize that hyperphysiologic mechanical loading leads to the accumulation of altered epigenetic markers in articular chondrocytes, resulting in a loss of the tightly regulated balance of gene expression that leads to a dysregulated state characteristic of the OA disease state.

Results

We showed that hyper-physiological loading evokes consistent changes in CpGs associated with expression changes (ML-tCpGs) in *ITGA5*, *CAV1*, and *CD44*, among other genes, which together act in pathways such as anatomical structure morphogenesis (GO:0009653) and response to wound healing (GO:0042060). Moreover, by comparing the ML-tCpGs and their associated pathways to tCpGs in OA pathophysiology (OA-tCpGs), we observed a modest but particular interconnected overlap with notable genes such as *CD44* and *ITGA5*. These genes could indeed represent lasting detrimental changes to the phenotypic state of chondrocytes due to mechanical perturbations that occurred earlier in life. The latter is further suggested by the association between methylation levels of ML-tCpGs mapped to *CD44* and OA severity.

Conclusion

Our findings confirm that hyper-physiological mechanical cues evoke changes to the methylome-wide landscape of chondrocytes, concomitant with detrimental changes in positional gene expression levels (ML-tCpGs). Since *CAV1, ITGA5*, and *CD44* are subject to such changes and are central and overlapping with OA-tCpGs of primary chondrocytes, we propose that accumulation of hyper-physiological mechanical cues can evoke long-lasting, detrimental changes in set points of gene expression that influence the phenotypic healthy state of chondrocytes. Future studies are necessary to confirm this hypothesis.

Introduction

Osteoarthritis (OA) is a complex, age-related multifactorial degenerative disease of the diarthrodial joints marked by impaired mobility, joint stiffness, pain, and a significant decrease in quality of life. Among other risk factors, such as genetics and age, hyper-physiological mechanical cues are known to play a critical role in the onset and progression of the disease (1). OA is characterized by an imbalance in the articular chondrocytes' anabolic and catabolic activities, impacting the integrity of the cartilage. Hyper-physiologic mechanical loading as seen with post-traumatic injury is compress articular chondrocytes and introduce catabolic signalling in chondrocytes (1, 2).

Previous studies have characterized the deregulated signalling pathways in articular chondrocytes in response to hyper-physiological mechanical cues with transcriptome-wide differential expression analyses. These studies show that hyper-physiologic mechanical cues significantly enhance cell apoptosis (3) and cellular senescence (4), increase catabolic gene expression (5), and reduce matrix production (6), whereas physiologic mechanical loading induces a broad anabolic response in the transcriptome that is associated with increased matrix formation (7). Post-mitotic cells, such as articular chondrocytes, heavily rely on methylation at CpG sites to adapt to environmental cues and maintain phenotypic plasticity (8). However, these long-lasting adaptations may eventually have a negative impact on cellular performance (9, 10). We hypothesize that hyper-physiologic mechanical loading leads to the accumulation of altered epigenetic markers in articular chondrocytes resulting in a loss of the tightly regulated balance of gene expression to a dysregulated state characteristic of the OA disease state.

Here, we aimed to study the effect of hyper-physiological mechanical stress on changes in DNA methylation-driven set points of epigenetically regulated gene expression that potentially contribute to OA-related loss of the chondrocytes' epigenetically controlled healthy maturational arrested phenotypic state. To this end, we employed an established human induced pluripotent stem cell (hiPSC)-derived cartilage organoid model and studied the methylome and transcriptome-wide changes in response to previously assessed hyper-physiological mechanical loading conditions (11). Using these techniques, we show that changes in the epigenetic set point of transcription in chondrocytes responding to hyper-physiological loading overlap with OA pathophysiology, further underlining their mutual role in evoking aberrant chondrocyte cellular functions.

Results

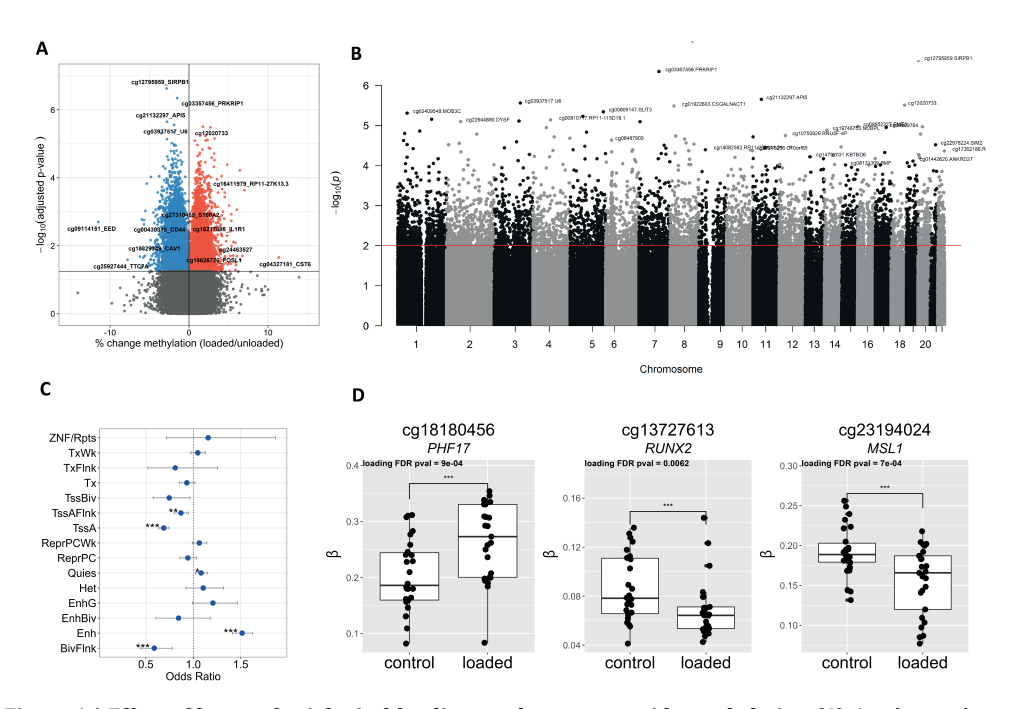


Figure 1 | Effect of hyper-physiological loading on the genome-wide methylation (A) A volcano plot of the methylome-wide response to hyper-physiological loading conditions. Red dots denote CpG sites mapped to a gene body with increased methylation, FDR<0.01, and blue dots represent CpG sites mapped to a gene body that are de-methylated in response to hyper-physiological loading conditions as determined by MEAL. (B) Manhattan plot of differentially methylated CpG sites with their genomic mapped genes. The horizontal red line represents the FDR<0.05 threshold. (C) Enrichment of significant DMs within chromatin states; active transcription start site (TSS), proximal promoter states (TssA, TssAFInk), a transcribed state at the 5' and 3' ends of genes showing both promoter and enhancer signatures (TxFInk), actively transcribed states (Tx, TxWk), enhancer states (Enh, EnhG), and a state associated with zinc finger protein genes (ZNF/Rpts). The inactive states consist of constitutive heterochromatin (Het), bivalent regulatory states (TssBiy, BivFlnk, EnhBiv), repressed Polycomb states (ReprPC, ReprPCWk), and a quiescent state (Quies) (D) Notable example of differentially methylated mapped CpGs in response to hyper-physiological mechanical loading conditions. The box plots represent the 25th, 50th, and 75th percentiles, and whiskers extend to 1.5 times the interquartile range. Individual samples are depicted by black dots in each graph. *FDR<0.05, **FDR<0.01, ***FDR<0.001.

Characterization of experimental set-up to test the epigenome- and transcriptome-wide effects of hyper-physiological loading.

To test the effects of hyper-physiological loading on the epigenetically regulated transcriptome, we employed a human induced pluripotent stem cell (hiPSC)-derived neo-cartilage organoid model. hiPSCs were differentiated into chondrocytes using a previously established chondrogenic differentiation protocol (12). To study the response of chondrocytes to hyper-physiological mechanical loading conditions we have applied two different models that are commonly used in osteoarthritis research: (1) chondrocyte derived (spherical) neo-cartilage constructs, and (2) chondrocytes embedded in (cylindrical) agarose constructs. To distill the most consistent effects we

employed both models and performed a meta-analysis on the methylome-wide changes in response to hyper-physiological mechanical loading. Successful differentiation towards chondrocytes and the production of neo-cartilage was confirmed by protein immunolabeling of collagen II (COLII) and collagen VI (COLVI), as well as staining for sulfated glycosaminoglycans (sGAGs) (Fig. S1A).

To test the hypothesis that injurious mechanical stress can alter the epigenetically regulated transcriptome, both of the organoid models were exposed to hyperphysiologic mechanical loading (total n=26) alongside unloaded controls (total n=27) (11). Methylome- and transcriptome-wide profiles resulting from the jointly analyzed neo-cartilage models, together with real-time quantitative polymerase chain reaction (RT-qPCR), immunohistochemistry (IHC), and dimethyl methylene blue (DMMB) assays, resulting from the spherical neo-cartilage organoids were measured 12 hours after mechanical stimulation. First, we characterized the response of neo-cartilage organoids to hyper-physiological loading conditions by targeted analysis using RT-qPCR of catabolic and anabolic cartilage markers and mechano-sensors (Table 1). Similar to other mechanically induced injurious in vitro and in vivo models of OA (4, 13), expression of anabolic ADAMTS5 significantly increased in response to hyper-physiological loading. This finding suggests that hyper-physiological loading conditions induced a catabolic response in neo-cartilage organoids. Additionally, there was an increase in PIEZO1 expression, which is hypothesized one of the main transducers of hyper-physiological mechanical loading (14). Nonetheless, staining intensity of COLII and COLVI, as well as sGAG deposition normalized to DNA content, showed no significant change in response to hyper-physiological loading conditions (Fig. S1B-C).

Methylome-wide response to hyper-physiological mechanical loading conditions

Following Illumina EPIC array analyses and quality control (QC), we obtained robust methylation data of 807655 CpGs for the two models to determine differential DNA methylation in response to hyper-physiological loading by meta-analysis. In total, we detected 6830 differentially methylated (DM) CpG sites (FDR<0.01, **Fig. 1A; Table S1)** and plotted them across the genome annotated with the GENCODE basic V12 database (**Fig. 1B**) (*15*). Notable examples of highly significant DM CpG sites are cg27310485 annotated to calcium binding protein S100A2 (beta = .01, FDR = $7.8X10^{-4}$), cg16217885 annotated to inflammatory receptor IL1R1 (beta = 0.01, FDR = $1.2x10^{-3}$), cg12795959 annotated to SIRPB1 (beta = -0.03, FDR = $2.4x10^{-7}$). As shown in **Fig. 1B**, we recognized some skyscrapers suggesting differentially methylated regions (DMRs). Upon defining DMRs as 3 or more DM CpGs with an inter-CpG distance of <1kb and allowing for 3 non-DM CpGs in the complete DMR (*16*), these DMRs did not reach statistical significance. To gain insight into the functional aspects of DM CpGs, their

enrichment to chromatin states was analyzed (*17*). As shown in **Fig. 1C**, DM CpG sites with hyper-physiological loading were significantly enriched within chromatin regions associated with active transcription start site (TSS) proximal promoter states TssAFlnk (OR=0.87, FDR=1.8X10⁻³), transcription start sites (TssA) (OR=0.69, FDR=4.7X10⁻²¹), enhancer states (Enh) (OR=1.51, FDR=6.5X10⁻³¹), bivalent regulatory states (BivFlnk) (OR=0.59, FDR=2.0X10⁻⁴), and a quiescent state (Quies) (OR=1.08, FDR=6.3X10⁻³). The highly significant enrichment for DM CpGs in Enh suggests that mechanical loading induced differential methylation, particularly at CpG sites that reside in genomic regions involved in the regulation of gene expression. Notable examples of highly significant DM CpG sites that mapped to such regulatory regions of gene expression were cg18180456 annotated *PHF17* encoding Jade Family PHD Finger 1 involved in histone acetylation (beta=-0.0632, FDR=8.8X10⁻⁵), cg13727613 annotated *RUNX2* encoding a well-known transcription factor detrimental to cartilage, (beta=-0.021,

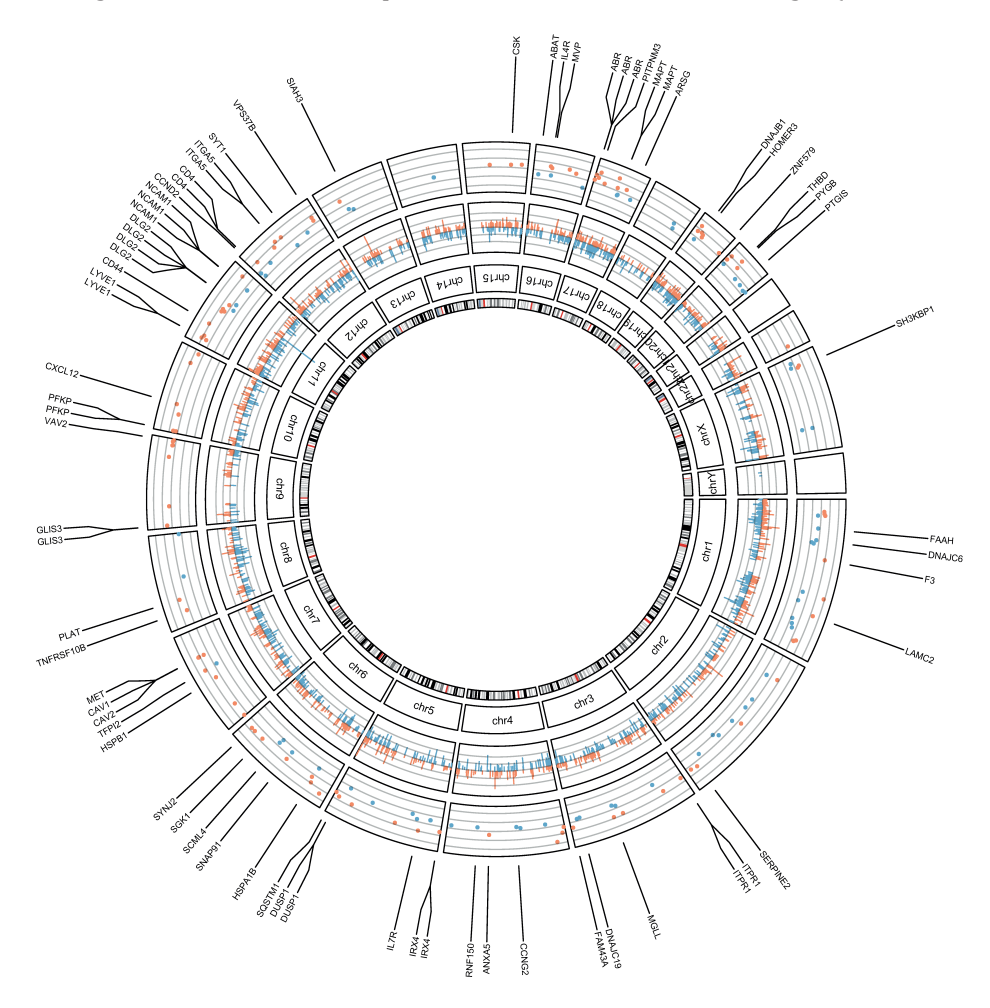


Figure 2 | Circos Plot of Transcriptionally active DM CpG sites responding to hyper-physiologic mechanical loading showing the genomic distribution of the DM CpG sites and positional DE genes. The inner circle displays the chromosomes. The middle circle displays change in percentage of the methylation of the 2492 DM-CpG's that mapped to a gene site. Blue bars depict de-methylated CpG-sites, red bars depict increased Methylated CpG-sites. (FDR<0.01) The outside circle displays the ²log fold change of the 169 unique DE ML-tCpG-Genes. Blue dots depict downregulation, red dots depict upregulation. (FDR<0.05)

FDR= $6.2X10^{-4}$), and cg23194024 annotated *MSL1* encoding a component of the histone acetyltransferase complex responsible for the majority of histone H4 acetylation (beta=0.032, FDR= $6.9X10^{-5}$) (Fig. 1D).

Transcriptionally active CpG-sites

To biologically interpret the DM CpG sites in response to hyper-physiological loading more specifically, we next integrated a previously assessed RNA sequencing dataset (18) of the same experiment. To prioritize DM CpG that likely affect gene expression, we first prioritized, among the DM CpG sites, those that mapped to genes within 200 or 1500 bp of the transcription start site (TSS200, TSS1500), located within the 3' or 5' UTR regions, or CpG sites that were exon bound. This resulted in 2492 CpG-gene pairs. (Fig. 2: Table S2). As shown in Figure 2. around multiple genes such as ITGA5. DLG2 and ABR multiple DM-CpGs are clustered. Next, among the 2492 DM CpG sites, we prioritized those that mapped to a gene that was also differentially expressed in response to hyper-physiological loading conditions based on FDR correction for the number of genes overlapping with mapped CpGs. This selection of the most likely transcriptionally active DM CpGs, henceforth defined as mechanical loading induced, transcriptionally active CpGs (ML-tCpGs), consisted of a total of 208 ML-tCpGs that mapped at TSS200 (15.4%), TSS1500 (28.5%), 3'UTR (13.65%), 5'UTR (32.2%), and 1st Exon (5.78%) or were Exonbound (4.3%) (Table S3). As shown in Fig. 2 and Table S3, these 208 MLtCpGs were connected to 169 unique differentially expressed (DE) genes. As shown in **Fig. 3A**, 57 of the 169 genes showed a strong protein-protein interaction (FDR = 2.4×10^{-1} 5) as determined by STRING-DB. Examples of highly connected ML-tCpGs-genes within this network are HSPA1B, CD44, and CAV1 (Fig. 3B-C). To gain insight into the biological processes that are affected by the ML-tCpGs responding to hyper-physiological loading conditions, we performed pathway enrichment analysis of gene ontology biological processes (GO BP), KEGG, and Reactome (Table S4) on all 169 unique genes that were associated with a ML-tCpG. Pathways such as anatomical structure morphogenesis (e.g., ANGPTL4, WNT9A, HMGA2), wound healing (e.g., HSPB1, SERPINE2, FERMT1), and caveola assembly (e.g., CAV1, CAV2, PACSIN2) were enriched.

Overlapping key nodes in the network of t-CpGs affected by mechanical loading and OA pathophysiology

To explore the role of the identified ML-tCpG-gene pairs in OA pathophysiology, we examined the overlap of our ML-tCpG-gene pairs with those previously reported tCpG-

gene pairs associated to OA pathophysiology, i.e. differentially expressed between lesioned and preserved cartilage from OA patients who underwent a joint replacement surgery (19). Although, the overlap was modest (n = 8 of 142 OA-tCpG-gene pairs) (Fig. S3), the ML-tCpG genes that did overlap with OA-tCpGs, *CD44*, *ITGA5*, and *CAV1*, are central and particularly interconnected genes in the network of both ML-tCpG-gene

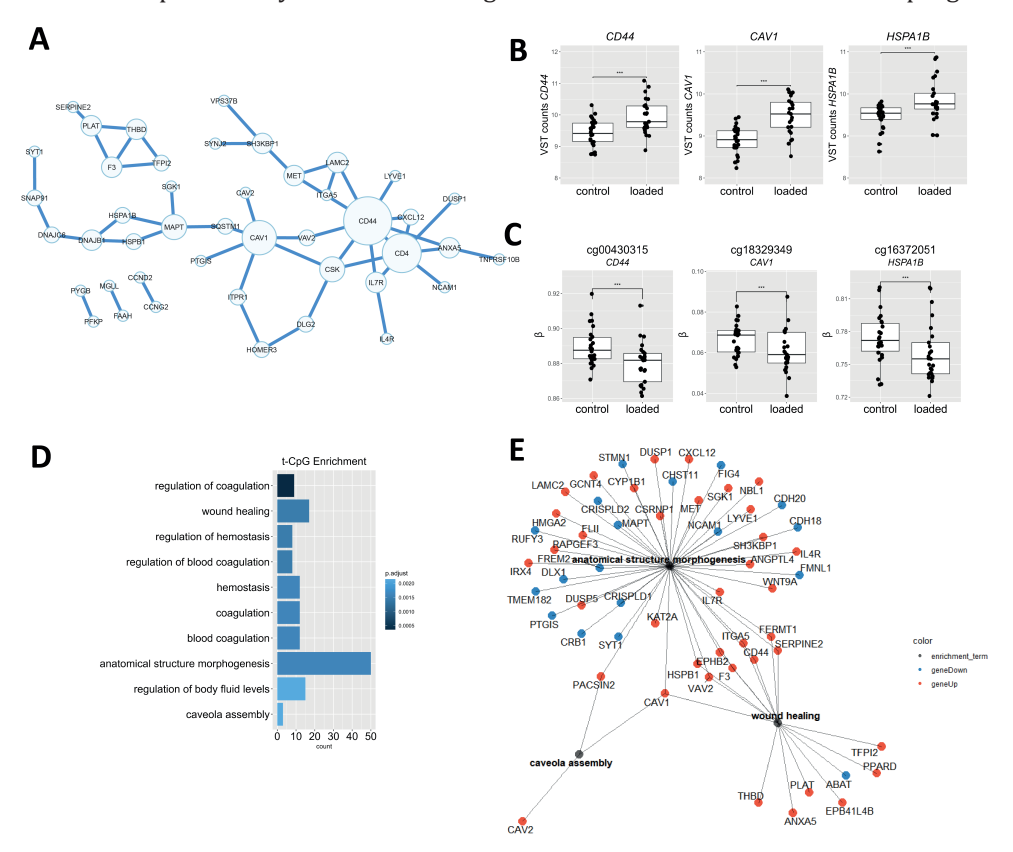


Figure 3 | **Epigenetically regulated transcriptome pathway enrichment analysis. (A)** Protein-protein network of ML-tCpG – genes as determined by STRING-DB. **(B)** Differential gene expression of genes to which a DM CpG was mapped. **(C)** Differential methylation of CpG sites mapped to the gene body. The box plots represent 25th, 50th, and 75th percentiles, and whiskers extend to 1.5 times the interquartile range. Individual samples are depicted by black dots in each graph. *FDR<0.05, ***FDR<0.001. **(D)** Top 10 most significantly enriched pathways of epigenetically regulated DEG. FDR<0.05. **(E)** Gene-pathway network of notable enriched pathways where lines depict the relationship between the genes and the pathways determined by enrichment analysis. Blue dots depict downregulated DEGs in response to hyper-physiologic mechanical loadings conditions, and red dots depict upregulated DEGs in response to hyper-physiologic mechanical loading conditions.

pairs and OA-tCpG-gene pairs (Fig. 3A; Fig. S2). Taken together, we showed that hyperphysiological loading resulted in changes in tCpG-gene pairs that are both located within gene regulatory chromatin states and that are central and responsive to changes that occur during OA pathophysiology.

Correlation of tCpGs with clinical OA phenotypes

Finally, we set out to gain insight into the clinical relevance of altered epigenetic control of the identified ML-tCpG. Therefore, we determined the association of ML-tCpGs overlapping with OA-related epigenetically regulated genes (8) to phenotypic traits in the respective preoperative radiograph of the OA patient (the RAAK study). This subset of ML-tCpGs was regulating *PFKP*, *CD44*, *CAV1*, *SVIL*, and *CY1BP1*. Next, to assess how methylation levels of these genes relate to OA severity, methylation levels in preserved cartilage from joint replacement surgeries of these overlapping ML-tCpGs were correlated with OA severity as determined by the Kellgren-Lawrence grading scale (KL-score), adjusted for BMI and age. We found that both *CD44* (beta=-0.053, P=0.048) and *PFKP* (beta=-0.111, P=3.12X10⁻³) methylation levels were negatively associated with the KL-score, suggesting indeed that mechanical loading-induced alterations in epigenetic set points of expression are associated to the OA disease state of the patient.

Discussion

The goal of this study was to determine the effect of hyper-physiological mechanical loading on changes in stable set points of epigenetically regulated gene expression (MLtCpGs) that could contribute to the long-lasting, detrimental changes in chondrocytes that are characteristic of an OA phenotype. To this end, we employed two human induced pluripotent stem cell (hiPSC)-derived neo-cartilage organoid models for robust readouts and studied the methylome- and transcriptome-wide changes in response to hyper-physiological mechanical loading conditions. We showed that hyper-physiological loading evokes consistent changes in ML-tCpGs associated with expression changes in ITGA5, CAV1, and CD44, among other genes, which together act in pathways such as anatomical structure morphogenesis (GO:0009653) and response to wound healing (G0:0042060). Moreover, by comparing the ML-tCpGs and their associated pathways to tCpGs in OA pathophysiology, we observed a modest but particular interconnected overlap with notable genes such as CD44 and ITGA5. These genes could indeed represent lasting detrimental changes to the phenotypic state of chondrocytes due to mechanical perturbations that occurred earlier in life. The latter is further suggested by the association between methylation levels of ML-tCpGs mapped to CD44 and OA severity.

Since injurious mechanical loading is considered an important driver of the onset and progression of the OA, here, we studied for the first time whether injurious mechanical loading evokes stable, detrimental changes to chondrocyte phenotypic states. In doing so, we revealed that DM CpGs are particularly enriched in transcription start sites and enhancers suggesting that the DM CpG sites evoke changes in gene transcription. However, we cannot exclude the epigenetic regulatory effects of *in trans* t-CPGs. To allow

biological interpretation of the DM CpGs in response to hyper-physiological loading, we integrated RNA sequencing data from the same experiment. We showed that significant differential CpG-gene pairs with hyper-physiological loading occurred, particularly near genes OA relevant genes (e.g., *ITGA5, CD44, CAV1, WNT9A,* and *HMGA2*). The relevance of mechanically induced expression of *ITGA5* is that the binding of matrix fragments such as fibronectin to integrin α5β1 heterodimer activates a pro-catabolic response (20). Also, *CD44* plays a role in matrix catabolism by degrading hyaluronic acid in articular cartilage (21), while catabolic stress has been shown to upregulate *CAV1*, coding for caveolin-1, which has been linked to chondrocyte senescence (22). Genes like *WNT9A* as well as *HMGA2* are reported OA risk genes (23). Nonetheless, the design of our study does not justify a direct causal relationship between DM at ML-CpGs and differential gene expression. To further confirm a direct causal relationship between CpG-specific methylation levels and gene expression, a CRISPR-Cas9-DNMT/TET1 guided manipulation of methylation levels of the identified CpG sites mapped to *CD44*, *PFKP*, *SVIL*, and *CY1BP1*, is warranted.

Here we have combined genome-wide methylation and RNAseq analysis of hiPSCderived chondrocytes either in deposited (spherical) neo-cartilage or embedded in (cylindrical) agarose, which currently are the most commonly used models in osteoarthritis research (7, 11, 14, 24). The advantage of the spherical neo-cartilage model is that it contains an extracellular matrix deposited by the chondrocytes. Herein the response of the chondrocyte to the mechanical perturbation likely reflects changes in the chondrocyte-matrix interaction. Additionally, it allows for evaluating responses of mechanical loading on sGAGs and other matrix constituents by histology. Henceforth, this model has been used to evaluate the effects of hyper-physiologic mechanical loading conditions on matrix properties. On the other hand, the strain distribution on the spherical pellets, hence chondrocytes, is less equal and could have reduced power or introduce bias. The advantage of the cylindrical-shaped model, for that matter, allows for an equal strain distribution, hence a more precise relation between the applied stress and the response of the chondrocytes to the deformation. By performing a metaanalysis on the methylome-wide landscape of these two models we aimed to distill the most consistent and robust effects in the molecular response to hyper-physiologic mechanical loading conditions.

Founded by the notion that early environmental challenges could evoke long-lasting changes to methylation at tCpG sites, resulting in detrimental changes to set points of gene expression, we sought evidence that ML-tCpGs are associated with previously assessed, OA-related differences in methylation in articular cartilage (OA-tCpGs) (8). We showed that genes such as *CAV1*, *CD44*, and *ITGA5* appeared to be identically changed,

highly interconnected, and central to both the OA-tCpGs and ML-tCpGs networks. As such, it is tempting to suggest that mechanical injurious loading can indeed contribute to stable and detrimental changes to the phenotypic state of chondrocytes eventually making the chondrocyte prone to an OA phenotype. Nonetheless, this hypothesis needs to be further investigated by confirming that *CD44* upregulation leads to detrimental downstream effects of chondrocytes towards an OA chondrocyte phenotype.

After subjecting the neo-cartilage organoids to a single episode of mechanical injurious loading, the epigenetic and transcriptomic profiles were captured 12 hours later. This loading regime was based on a previous study, which optimized the loading regime to induce catabolic signaling in neo-cartilage organoids. (11) Although this loading regime resulted in many changes in methylation and associated expression, we did not observe changes in matrix content. The fact that histological changes were not visible is likely due to the relatively early time point and/or the intrinsic insensitivity of identifying changes in protein levels. Moreover, although changes in methylation at CpG sites are generally considered stable and long-lasting (10), the fact that we only measured methylation at 12 hours post-stimulus did not allow us to confirm the duration of the change in methylation, and future studies may wish to address this question directly. Additionally, this model of hyper-physiological loading in hiPSC neo-cartilage organoids can be expanded to define and apply more beneficial mechanical loading regimes, further unraveling the shift in molecular mechanisms underlying the normal physiological response to loading, and potentially counteract the detrimental changes in set-points in gene expression as induced by more damaging loading regimes. Such insights might further aid in the development of treatment strategies.

Conclusion

Together, the current study confirms that hyper-physiological mechanical cues evoke changes to the methylome-wide landscape of chondrocytes, concomitant with detrimental changes in positional gene expression levels (ML-tCpGs). Since *CAV1*, *ITGA5*, and *CD44* are subject to such changes and are central and overlapping with OA-tCPGs of autologous cartilage, we advocate that accumulation of hyper-physiological mechanical cues can evoke long-lasting, detrimental changes in set points of gene expression that eventually affect the phenotypic healthy state of chondrocytes. Future studies are necessary to confirm this hypothesis.

Methods

Experimental design

The objective of the current study was to study the effects of hyper-physiologic

mechanical loading conditions on the epigenetically regulated transcriptome. Here, we employed an hiPSC-derived neo-cartilage organoid model that was exposed to hyperphysiological mechanical loading conditions. These samples were then analyzed using 850k EPIC array and RNA sequencing.

hiPSC line and cell culture

An hiPSC line as described earlier was used (12). In short, the RVR-hIPSC line was retrovirally reprogrammed from human foreskin BJ fibroblasts and characterized. The hiPSCs were maintained under standard conditions (37 °C, 5% CO₂) on Matrigel (Corning, cat # 356237, New York, US) coated plates and refreshed daily with TeSR-E8 medium (STEMCELL Technologies, Vancouver, Canada) with 0.5% penicillin-streptomycin (P/S; Gibco Landsmeer, the Netherlands) upon reaching approximately 70% confluence.

hiPSC differentiation to induced chondrocytes

Generation of hiPSC-derived chondrocytes was based on a protocol previously described (12), which was shown to result in the formation of tissue similar to young human cartilage (25-27). When hiPSCs reached 60% confluence, the culture medium was switched to mesodermal differentiation (MD) medium, composed of IMDM GlutaMAX (IMDM; Thermo Fisher Scientific, St Louis, MO) and Ham's F12 Nutrient Mix (F12; Sigma-Aldrich Zwijndrecht, the Netherlands) with 1% chemically defined lipid concentrate (Gibco Landsmeer, the Netherlands), 1% insulin/human transferrin/selenous (ITS+; Corning), 0.5% penicillin-streptomycin (P/S; Gibco Landsmeer, the Netherlands), and 450 μM 1-thioglycerol (Sigma-Aldrich, Zwijndrecht, the Netherlands). Before induction of anterior primitive streak (day 0), hiPSCs were washed with wash medium (IMDM/ F12 and 0.5% P/S) and then fed with MD medium supplemented with activin A (30 ng/ml; Stemgent), 4 μM CHIR99021 (CHIR; Stemgent, Zwijndrecht, the Netherlands), and human fibroblast growth factor (20 ng/ml; FGF-2; R&D Systems) for 24 hours. Subsequently, the cells were washed again with wash medium, and paraxial mesoderm was induced on day 1, by MD medium supplemented with 2 μM SB-505124 (Tocris, Bristol, United Kingdom, 3 µM CHIR, FGF-2 (20 ng/ml), and 4 µM dorsomorphin (Tocris, Bristol, United Kingdom for 24 hours. Before induction of early somite (day 2), cells were washed with wash medium, and then cells were fed with MD medium supplemented with 2 μM SB-505124, 4 μM dorsomorphin, 1 μM C59 (Cellagen Technology), and 500 nM PD173074 (Tocris, Bristol, United Kingdom), for 24 hours. Subsequently, cells were washed with wash medium, and for induction of sclerotome, cells (days 3 to 5) were fed daily with MD medium supplemented with 2 μM purmorphamine (Stemgent Zwijndrecht, the Netherlands) and 1 µM C59. To induce chondroprogenitor cells (days 6 to 14), cells were washed briefly with wash medium and fed daily with MD medium supplemented with human bone morphogenetic protein 4 (BMP-4; 20 ng/ml; Miltenyi

Biotec, Leiden, The Netherlands).

Monolayer cultured hiPSC aggregates present at day 14 of the differentiation were washed with MD medium, dissociated with Gentle Cell dissociation medium (Stem Cell, Vancouver, Canada) and centrifuged for 5 min at 300G. Cell aggregates were subsequently maintained in chondrogenic differentiation (CD) medium containing Dulbecco's modified Eagle's medium/F12 (Gibco Landsmeer, the Netherlands, supplemented with 1% ITS+, 55 μM 2-mercaptoethanol (Gibco Landsmeer, the Netherlands), 1% nonessential amino acids (Gibco Landsmeer, the Netherlands), 0.5% P/S, L-ascorbate-2-phosphate (50 $\mu g/ml$; Sigma-Aldrich , Zwijndrecht, the Netherlands), ML329 (1 μM ; CSNpharm), C59 (1 μM ; Tocris , Bristol, United Kingdom),, and transforming growth factor- $\beta 3$ (10 ng/ml; PeproTech, Londen, United Kingdom) for 30 days while refreshing medium every 3 to 4 days.

Neo-cartilage organoid models

Two different chondrogenic constructs were used for downstream analysis; either these chondrogenic constructs were directly used for further experiments or they were dissociated using collagenase II, encapsulated in 2% w/v agarose at 30 million cells/ml, and cultured for 14 days with CD creating cylindrical shaped constructs. Across the independent differentiations a total of 53 samples were used for molecular profiling via RNA-seq and Methylation analysis divided loaded samples (n=26) alongside unloaded controls (n=27).

Mechanical loading

The spherical shaped neo-cartilage constructs were mechanically loaded using a MACH-1 mechanical testing device (Biomomentum, Laval, Canada), at a rate of 5hz with 20% sinusoidal peak-to-peak strain for 10 minutes as described earlier (11). The cylindrical constructs were loaded with a custom-build mechanical loading device, with the same loading regime. After mechanical loading, we have placed the neo-cartilage organoids back into CD medium excluding transforming growth factor- β 3 to prevent interference of its anabolic response with the response to mechanical loading.

sGAG measurement

Sulphated glycosaminoglycan (sGAG) concentrations in the neo-cartilage organoids (μg sGAG/μg DNA) was measured using the Farndale Dimethyl Methylene Blue (DMMB, Sigma, Zwijndrecht, the Netherlands) method (28). Chondroitin sulphate (Sigma, Zwijndrecht, the Netherlands) was used as a reference standard. Absorbance was measured at 535 and 595 using a microplate reader (Synergy HT, Biotek, Winooski,

VT, USA). Neo-cartilage sGAG concentrations were corrected for DNA content measured with the Qubit® 2.0 Fluorometer (Invitrogen™, Carlsbad, CA, USA) using the dsDNA HS Assay Kit (Invitrogen™, Carlsbad, CA, USA).

Histology and immunohistochemistry

Neo-cartilage samples were fixed in 4% formaldehyde and embedded in paraffin. Sections were stained with Alcian Blue (Sigma-Aldrich, Zwijndrecht, the Netherlands) and Nuclear Fast Red (Sigma-Aldrich, Zwijndrecht, the Netherlands). Deposition of collagen VI and collagen II in the neo-cartilage constructs was visualized immunohistochemically using a polyclonal antibody for COL6A1 (abcam ab6588), a primary sub-unit of COLVI, and a polyclonal antibody for COL2A1 (abcam ab34712), a primary sub-unit of COLII., antigen retrieval was done by treating deparaffinized sections with proteinase K (5 $\mu g/$ ml, Qiagen Venlo, the Netherlands) and hyaluronidase (5 mg/ml, Sigma Zwijndrecht, the Netherlands). Sections were incubated overnight with the primary antibodies, followed by incubation with a HRP conjugated secondary antibody (ImmunoLogic). Peroxidase binding for collagen VI was visualized using diaminobenzidine, and sections were counterstained with haematoxylin.

RT-qPCR

Per sample, two replicate neo-cartilage pellets were collected in TRIzol (Invitrogen™, Carlsbad, CA, USA), and RNA was isolated using the RNeasy Mini Kit (Qiagen, Venlo, the Netherlands) according to the manufacturer's protocol. DNA contamination was removed by treating the RNA with Rnase-Free DNase. RNA quality (A260/280: 1.7-2.0) was assessed using a nanodrop. RNA concentrations were measured with the Qubit® 2.0 Fluorometer (Invitrogen™, Carlsbad, CA, USA) using the RNA HS Assay Kit (Invitrogen[™], Carlsbad, CA, USA), with an A260/280 between 1.7-2.0. RNA was reverse transcribed into cDNA using the Transcriptor First Strand cDNA Synthesis Kit (Roche, Basel, Switzerland). cDNA was amplified using FastStart SYBR Green Master (Roche, Basel, Switzerland), and mRNA expression was measured in triplicates in a MicroAmp™ Optical 384-Well Reaction Plate (ThermoFisher Scientific, Landsmeer, the Netherlands), using the QuantStudio™ Flex Real-Time PCR system (Applied Biosystems™, Foster City, CA, USA), with the following cycling conditions: 10 min 95 °C; 10 sec 95 °C, 30 sec 60 °C, 20 sec 72 °C (45 cycles); 1 min 65 °C and 15 sec 95 °C. Primer efficiency was tested using a cDNA dilution series, and primers were considered efficient with an efficiency between 90% and 110%. -ΔCt expression levels were calculated using two housekeeping genes GAPDH and SDHA with the following formula: $\Delta Ct = Ct$ (gene of interest) - Ct (average housekeeping genes). Both housekeeping genes were stably expressed in this model. Fold changes were calculated using the 2-DACt method with $\triangle \Delta Ct = \triangle Ct \ (MS) - \triangle Ct \ (Control).$

Methylation data analysis

DNA methylation was assessed using the Illumina Infinium Methylation EPIC (850K) BeadChip according to GenomeScan's standard operating procedures (SOPs) based on the Illumina Infinium II Protocol. To analyze methylation array data (MethylationEPIC 850k array), the MethylAid R script (29)All samples showed a detected CpG above 95%. The minfi.v_1.36.0 R package (30) was used to pre-process the data. We removed any probe that have failed in one or more samples (p < 0.01). Probe level intensities were quantile normalized across samples prior to calculation of the \(\mathbb{G}\)-values. MethylToSNP was used to filter SNPs. This method looked for patterns in methylation array data and identified methylation probes with SNP-like patterns. The method removes outliers, which adds robustness to the analysis and is enabled by default. A confidence score was calculated to show how close the observed pattern of methylation beta values was to a canonical case of a SNP in a homozygously methylated CpG locus. Additionally, MethylToSNP can overlap the SNPs identified in methylation data with known SNPs from dbSNP. The probes that have shown to be cross-reactive (demonstrated to map to multiple places in the genome) were filtered out (31). The probes that were overlapping with rare SNPs (probes in transcription factor binding sites that showed extreme methylation pattern) were filtered out (32). To minimize the unwanted variation within and between samples, we used the Functional Normalization method from the minfi.1.36.0 R package (33) We ran differential mean analysis using t-moderated statistics. Using the MEAL.1.20.3 R package pipeline, which, relies on the lmFit from limma R package (design model=~ Loading). CpGs after Bonferroni correction P < 6.243109e-08 (0.05/800883) were considered significant. Stratified analysis for each neo-cartilage construct was performed. These two datasets were then combined with a random effect meta-analysis using the metaVolcano R package The circos plot was produced using the Circlize 0.4.3 R package (34).

Statistical analysis

For all data analysis except methylome data, we have used a generalized linear model including the factors hyper-physiological loading using R statistical software version 4.1.1.

Declarations

Ethical Approval

Not applicable

Funding

Leiden University Medical Centre, Pfizer Groton, Connecticut, USA and the Dutch Arthritis

Society have supported the GARP study. Furthermore, the research leading to these results has received funding from the Biobanking and BioMolecular resources Research Infrastructure the Netherlands (BBMRI-NL) (complementation project CP2013-84), the Dutch Scientific Research council NWO/ZonMW VICI scheme (nr. 91816631/528) and the Dutch Arthritis Society. We are indebted to drs. N. Riyazi, J. Bijsterbosch, H.M. Kroon and I. Watt for collection of data. Furthermore, this work was supported by the Shriners Hospitals for Children and the NIH (grants AG46927, AG15768, AR080902, AR072999, AR073752, and AR074992). Additionally, the data is generated within the scope of the Medical Delta programs Regenerative Medicine 4D: Generating complex tissues with stem cells and printing technology and Improving Mobility with Technology. This publication is part of the LoaD project (NWA.1389.20.009) of the NWA-research program Research by Consortia (ORC) that is financed by the Netherlands Organisation of Scientific Research (NWO).

Author Contributions

N.G.C.B., A.R.D., Y.F.M.H. F.G., I.M. developed the concept of this study: N.G.C.B., Z.H., A.R.D., G.H. R.G.N. and F.G., acquired materials and data; N.G.C.B., Y.F.M.H, F.G. and I.M. analyzed the data; and all authors contributed to the writing of the manuscript.

Competing interests

None

Availability of Data and Materials

All data needed to evaluate the conclusions in the paper are present in the paper and/ or the Supplementary Materials. Additional data related to this paper may be requested from the authors.

References

- F. Guilak. Biomechanical factors in osteoarthritis. Best Pract Res Clin Rheumatol 25, 815-823 (2011).
- T. L. Vincent, Mechanoflammation in osteoarthritis pathogenesis. *Semin Arthritis Rheum* **49**, S36-S38 (2019).
 C. T. Chen, N. Burton-Wurster, C. Borden, K. Hueffer, S. E. Bloom, G. Lust, Chondrocyte necrosis and apoptosis in impact damaged articular cartilage. *J Orthop Res* **19**, 703-711 (2001).
- E. Houtman, M. Tuerlings, J. Riechelman, E. Suchiman, R. J. P. van der Wal, R. Nelissen, H. Mei, Y. F. M. Ramos, R. Coutinho de Almeida, I. Meulenbelt, Elucidating mechano-pathology of osteoarthritis: transcriptome-wide differences in mechanically stressed aged human cartilage explants. *Arthritis Res Ther* **23**, 215 (2021).

- J. H. Lee, J. B. Fitzgerald, M. A. Dimicco, A. J. Grodzinsky, Mechanical injury of cartilage explants causes specific time-dependent changes in chondrocyte gene expression. *Arthritis Rheum* **52**, 2386-2395 (2005).
 B. Kurz, M. Jin, P. Patwari, D. M. Cheng, M. W. Lark, A. J. Grodzinsky, Biosynthetic response and mechanical properties of articular cartilage after injurious compression. *J Orthop Res* **19**, 1140-1146 (2001).
 R. J. Nims, L. Pferdehirt, N. B. Ho, A. Savadipour, J. Lorentz, S. Sohi, J. Kassab, A. K. Ross, C. J. O'Conor, W. B. Liedtke, B. Zhang, A. L. McNulty, F. Guilak, A synthetic mechanogenetic gene circuit for autonomous drug delivery in engineered
- W. den Hollander, Y. F. Ramos, N. Bomer, S. Elzinga, R. van der Breggen, N. Lakenberg, W. J. de Dijcker, H. E. Suchiman, B. J. Duijnisveld, J. J. Houwing-Duistermaat, P. E. Slagboom, S. D. Bos, R. G. Nelissen, I. Meulenbelt, Transcriptional associations of osteoarthritis-mediated loss of epigenetic control in articular cartilage. Arthritis Rheumatol 67, 2108-2116 (2015).
- E. W. Tobi, J. J. Goeman, R. Monajemi, H. Gu, H. Putter, Y. Zhang, R. C. Slieker, A. P. Stok, P. E. Thijssen, F. Muller, E. W. van Zwet, C. Bock, A. Meissner, L. H. Lumey, P. Eline Slagboom, B. T. Heijmans, DNA methylation signatures link prenatal famine exposure to growth and metabolism. *Nat Commun* 5, 5592 (2014).
 B. T. Heijmans, E. W. Tobi, A. D. Stein, H. Putter, G. J. Blauw, E. S. Susser, P. E. Slagboom, L. H. Lumey, Persistent epigenetic

Mechanical loading alters epigenetic set-poins of gene expression levels

differences associated with prenatal exposure to famine in humans. *Proc Natl Acad Sci U S A* **105**, 17046-17049 (2008). R. G. M. Timmermans, N. G. C. Bloks, M. Tuerlings, M. van Hoolwerff, R. Nelissen, R. J. P. van der Wal, P. M. van der Kraan, A. B. Blom, M. H. J. van den Bosch, Y. F. M. Ramos, I. Meulenbelt, A human in vitro 3D neo-cartilage model to explore the response of OA risk genes to hyper-physiological mechanical stress. *Osteoarthr Cartil Open* 4, 100231 (2022). S. S. Adkar, C. L. Wu, V. P. Willard, A. Dicks, A. Ettyreddy, N. Steward, N. Bhutani, C. A. Gersbach, F. Guilak, Step-Wise

Chondrogenesis of Human Induced Pluripotent Stem Cells and Purification Via a Reporter Allele Generated by CRISPR-

Cas9 Genome Editing. *Stem Cells* **37**, 65-76 (2019).
S. S. Glasson, R. Askew, B. Sheppard, B. Carito, T. Blanchet, H. L. Ma, C. R. Flannery, D. Peluso, K. Kanki, Z. Yang, M. K. Majumdar, E. A. Morris, Deletion of active ADAMTS5 prevents cartilage degradation in a murine model of osteoarthritis. Nature 434, 644-648 (2005).

W. Lee, R. J. Nims, A. Savadipour, Q. Zhang, H. A. Leddy, F. Liu, A. L. McNulty, Y. Chen, F. Guilak, W. B. Liedtke, Inflammatory signaling sensitizes Piezo1 mechanotransduction in articular chondrocytes as a pathogenic feed-forward mechanism in

osteoarthritis. Proc Natl Acad Sci U S A 118, (2021).

- 15. A. Frankish, M. Diekhans, A. M. Ferreira, R. Johnson, I. Jungreis, J. Loveland, J. M. Mudge, C. Sisu, J. Wright, J. Armstrong, A. Frankish, M. Dieknans, A. M. Ferreira, K. Johnson, I. Jungreis, J. Loveland, J. M. Mudge, C. Sisu, J. Wright, J. Armstrong, I. Barnes, A. Berry, A. Bignell, S. Carbonell Sala, J. Chrast, F. Cunningham, T. Di Domenico, S. Donaldson, I. T. Fiddes, C. Garcia Giron, J. M. Gonzalez, T. Grego, M. Hardy, T. Hourlier, T. Hunt, O. G. Izuogu, J. Lagarde, F. J. Martin, L. Martinez, S. Mohanan, P. Muir, F. C. P. Navarro, A. Parker, B. Pei, F. Pozo, M. Ruffier, B. M. Schmitt, E. Stapleton, M. M. Suner, I. Sycheva, B. Uszczynska-Ratajczak, J. Xu, A. Yates, D. Zerbino, Y. Zhang, B. Aken, J. S. Choudhary, M. Gerstein, R. Guigo, T. J. P. Hubbard, M. Kellis, B. Paten, A. Reymond, M. L. Tress, P. Flicek, GENCODE reference annotation for the human and mouse genomes. Nucleic Acids Res 47, D766-D773 (2019).
- R. C. Slieker, S. D. Bos, J. J. Goeman, J. V. Bovee, R. P. Talens, R. van der Breggen, H. E. Suchiman, E. W. Lameijer, H. Putter, E. B. van den Akker, Y. Zhang, J. W. Jukema, P. E. Slagboom, I. Meulenbelt, B. T. Heijmans, Identification and systematic annotation of tissue-specific differentially methylated regions using the Illumina 450k array. *Epigenetics Chromatin* 6, 26
- R. E. C. I. a. c. K. A. M. W. E. J. B. M. 5, S. p. m. C. L. H. 53, P. i. B. B. E. C. J. F. E. J. R. H. M. M. A. M. A. R. B. 8, Integrative analysis of 111 reference human epigenomes. *Nature* 518, 317-330 (2015).
- N. G. C. Bloks, Z. Harissa, S. S. Adkar, A. Dicks, G. Hajmousa, N. Steward, R. I. Koning, A. Mulder, B. B. de Koning, M. Kloppenburg, A high-impact COL6A3 mutation alters the response of chondrocytes in neo-cartilage organoids to hyper-
- Physiologic mechanical loading. *bioRxiv*, (2022).

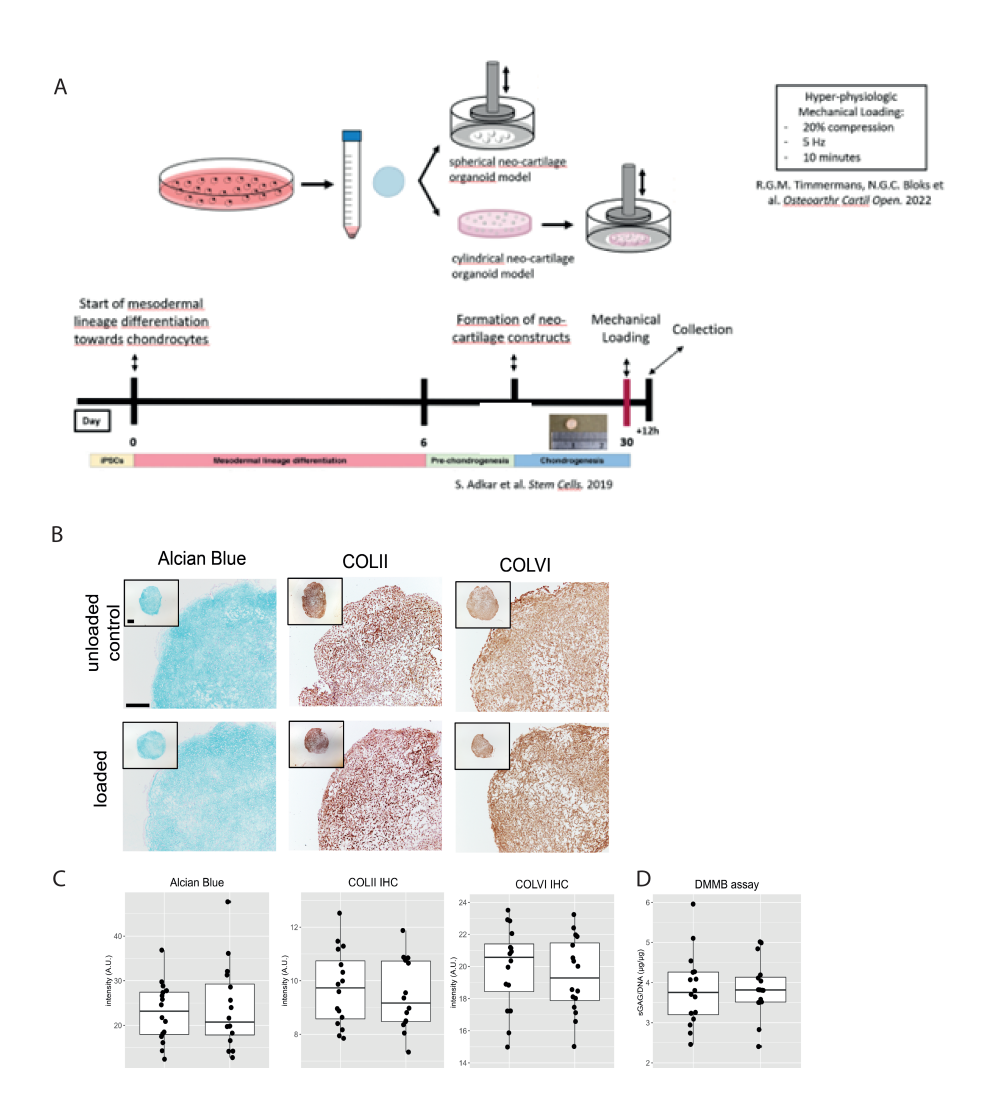
 R. Coutinho de Almeida, Y. F. M. Ramos, A. Mahfouz, W. den Hollander, N. Lakenberg, E. Houtman, M. van Hoolwerff, H. E. D. Suchiman, A. Rodriguez Ruiz, P. E. Slagboom, H. Mei, S. M. Kielbasa, R. Nelissen, M. Reinders, I. Meulenbelt, RNA sequencing data integration reveals an miRNA interactome of osteoarthritis cartilage. Ann Rheum Dis 78, 270-277 (2019).
- R. F. Loeser, Integrins and chondrocyte-matrix interactions in articular cartilage. Matrix Biol 39, 11-16 (2014)
- W. Knudson, G. Chow, C. B. Knudson, CD44-mediated uptake and degradation of hyaluronan. Matrix Biol 21, 15-23 (2002).
- Š. M. Ďai, Z. Z. Shan, H. Nakamura, K. Masuko-Hongo, T. Kato, K. Nishioka, K. Yudoh, Catabolic stress induces features of chondrocyte senescence through overexpression of caveolin 1: possible involvement of caveolin 1-induced downregulation of articular chondrocytes in the pathogenesis of osteoarthritis. Arthritis and Rheumatism 54, 818-831 (2006).
- regulation of articular chondrocytes in the pathogenesis of osteoarthritis. Arthritis and Rheumatism 54, 818-831 (2006).
 C. G. Boer, K. Hatzikotoulas, L. Southam, L. Stefansdottir, Y. Zhang, R. Coutinho de Almeida, T. T. Wu, J. Zheng, A. Hartley, M. Teder-Laving, A. H. Skogholt, C. Terao, E. Zengini, G. Alexiadis, A. Barysenka, G. Bjornsdottir, M. E. Gabrielsen, A. Gilly, T. Ingvarsson, M. B. Johnsen, H. Jonsson, M. Kloppenburg, A. Luetge, S. H. Lund, R. Magi, M. Mangino, R. Nelissen, M. Shivakumar, J. Steinberg, H. Takuwa, L. F. Thomas, M. Tuerlings, O. C. arc, H. A.-I. Pain, A. Consortium, C. Regeneron Genetics, G. C. Babis, J. P. Y. Cheung, J. H. Kang, P. Kraft, S. A. Lietman, D. Samartzis, P. E. Slagboom, K. Stefansson, U. Thorsteinsdottir, J. H. Tobias, A. G. Uitterlinden, B. Winsvold, J. A. Zwart, G. Davey Smith, P. C. Sham, G. Thorleifsson, T. R. Gaunt, A. P. Morris, A. M. Valdes, A. Tsezou, K. S. E. Cheah, S. Ikegawa, K. Hyeem, T. Esko, J. M. Wilkinson, I. Meulenbelt, M. T. M. Lea, L. R. L. van Meurs, H. Styrkarsdottir, F. Zergini, Deciphering esteoarthritis genetics across 876.690 individuals T. M. Lee, J. B. J. van Meurs, U. Styrkarsdottir, E. Zeggini, Deciphering osteoarthritis genetics across 826,690 individuals from 9 populations. *Cell* **184**, 4784-4818 e4717 (2021).
- M. van Hoolwerff, A. Rodriguez Ruiz, M. Bouma, H. E. D. Suchiman, R. I. Koning, C. R. Jost, A. A. Mulder, C. Freund, F. Guilak, Y. F. M. Ramos, I. Meulenbelt, High-impact FN1 mutation decreases chondrogenic potential and affects cartilage
- dulak, T. F. M. Ramos, I. Methenbert, Filgh-Impact FN1 mutation decreases choindrogenic potential and affects cartilage deposition via decreased binding to collagen type II. *Sci Adv* 7, eabg8583 (2021).

 A. Rodriguez Ruiz, A. Dicks, M. Tuerlings, K. Schepers, M. van Pel, R. Nelissen, C. Freund, C. L. Mummery, V. Orlova, F. Guilak, I. Meulenbelt, Y. F. M. Ramos, Cartilage from human-induced pluripotent stem cells: comparison with neocartilage from chondrocytes and bone marrow mesenchymal stromal cells. *Cell Tissue Res* 386, 309-320 (2021).

 C. L. Wu, A. Dicks, N. Steward, R. Tang, D. B. Katz, Y. R. Choi, F. Guilak, Single cell transcriptomic analysis of human pluripotent stem cell schondrogenesis. *Next Computer* 13, 262 (2021).
- Duripotent stem cell chondrogenesis. *Nat Commun* 12, 362 (2021).

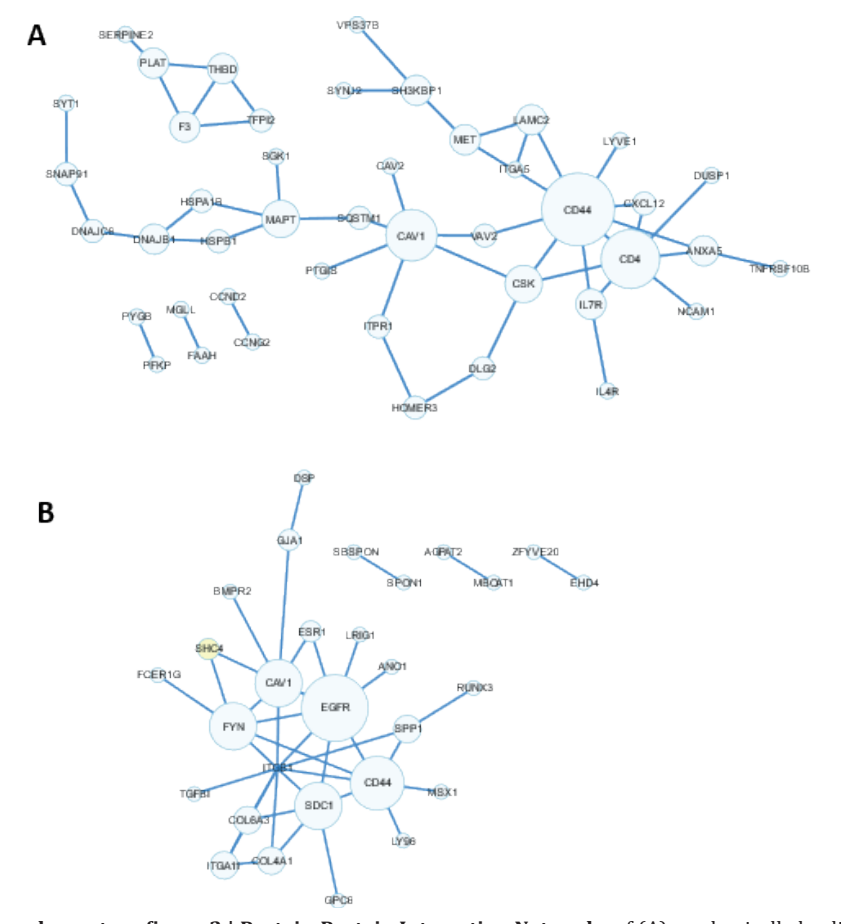
 A. Dicks, C. L. Wu, N. Steward, S. S. Adkar, C. A. Gersbach, F. Guilak, Prospective isolation of chondroprogenitors from
- human iPSCs based on cell surface markers identified using a CRISPR-Cas9-generated reporter. Stem Cell Res Ther 11, 66
- 28 R. W. Farndale, C. A. Sayers, A. J. Barrett, A Direct Spectrophotometric Microassay for Sulfated Glycosaminoglycans in Cartilage Cultures. Connective Tissue Research 9, 247-248 (1982).
- M. van Iterson, E. W. Tobi, R. C. Slieker, W. den Hollander, R. Luijk, P. E. Slagboom, B. T. Heijmans, MethylAid: visual and interactive quality control of large Illumina 450k datasets. *Bioinformatics* 30, 3435-3437 (2014).
- M. J. Aryee, A. E. Jaffe, H. Corrada-Bravo, C. Ladd-Acosta, A. P. Feinberg, K. D. Hansen, R. A. Irizarry, Minfi: a flexible and comprehensive Bioconductor package for the analysis of Infinium DNA methylation microarrays. *Bioinformatics* 30, 1363-1369 (2014).
- Y. A. Chen, M. Lemire, S. Choufani, D. T. Butcher, D. Grafodatskaya, B. W. Zanke, S. Gallinger, T. J. Hudson, R. Weksberg, Discovery of cross-reactive probes and polymorphic CpGs in the Illumina Infinium HumanMethylation450 microarray. Epigenetics 8, 203-209 (2013)
- A. Martin-Trujillo, N. Patel, F. Richter, B. Jadhav, P. Garg, S. U. Morton, D. M. McKean, S. R. DePalma, E. Goldmuntz, D. Gruber, R. Kim, J. W. Newburger, G. A. Porter, Jr., A. Giardini, D. Bernstein, M. Tristani-Firouzi, J. G. Seidman, C. E. Seidman, W. K. Chung, B. D. Gelb, A. J. Sharp, Rare genetic variation at transcription factor binding sites modulates local DNA methylation profiles. *PLoS Genet* **16**, e1009189 (2020).
- J. P. Fortin, T. J. Triche, Jr., K. D. Hansen, Preprocessing, normalization and integration of the Illumina Human Methylation EPIC array with minfi. Bioinformatics 33, 558-560 (2017).
- 30, 2811-2812 (2014).

Supplementary Figures

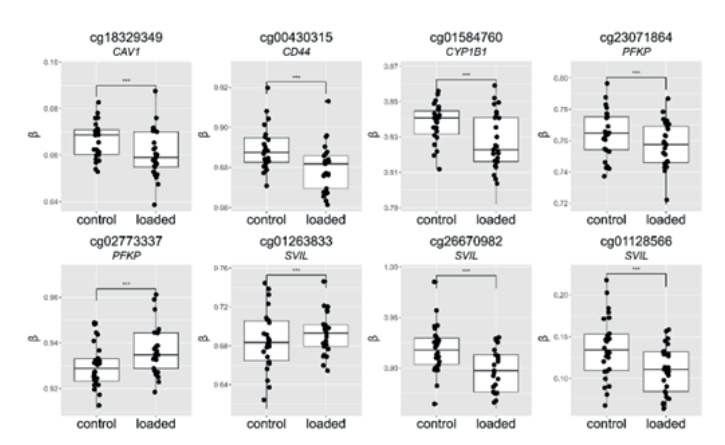


Supplementary figure 1 | Experimental set-up and effect of the hyper-physiological loading conditions on matrix deposition neo-cartilage organoids (A) Schematic representation experimental set-up adapted from Bloks et al. 2023, BioArxiv: hiPS cells were differentiated using an established differentiation protocol to produce neo-cartilage organoids. Two different organoid models were employed and jointly analyzed; 1. A spherical pellet model harnessing the original matrix produced by the hiPSCs. 2. A cylindrical organoid model in which the hiPSC-derived chondrocytes were embedded in an agarose construct, ideally suited for testing the effects of mechanical loading conditions. These constructs were both exposed to hyper-physiological loading conditions, after which the organoids were harvested for downstream analysis. (B)Representative images of Alcian blue staining marking sulfated glucosaminoglycans (sGAGs) and immunohistological stainings of collagen II (COL II) and collagen VI (COLVI) in spherical neo-cartilage organoids. Scale bar 200µm. (C) Quantification of Alcian blue, COLII, and COLVI in unloaded controls and loaded spherical neo-cartilage organoids show no significant effect of hyper physiological loading (N=16). (D) Quantification of SGAG deposition in neo-cartilage organoids is not affected by mechanical loading. (N=16). Statistics are reported as beta ± standard error. The box plots represent 25th,

50th, and 75th percentiles, and whiskers extend to 1.5 times the interquartile range. Individual samples are depicted by black dots in each graph. P values were attained using a generalized linear model, with intensity (for immuno-stainings) and (sGAGs/DNA) as dependent variable and genotype as independent variable.



Supplementary figure 2 | Protein-Protein Interaction Networks of (A) mechanically loading- or (B) OA-associated tCpGs as determined by STRING-DB.



Supplementary figure 3 | **Differential methylation of overlapping ML-tCpGs-genes with OA-tCpGs-genes.** Differential methylation of CpG sites mapped to the gene body. The box plots represent 25th, 50th, and 75th percentiles, and whiskers extend to 1.5 times the interquartile range. Individual samples are depicted by black dots in each graph. *FDR<0.05, ***FDR<0.001.

Supplementary Table S1 (partially) - Meta-analysis of differentially methylated CpG sites in response to mechanical loading in spherical and cylindrical neo-cartilage organoids (N=6830).

chr20 1569403 -2 2.37E-07 chr7 102067072 -2 4.53E-07 chr11 43355493 -2 2.24E-06 chr3 133383077 -2 2.76E-06 chr8 19504047 2 3.11E-06 chr8 19504047 2 3.28E-06 chr8 19504047 2 3.28E-06 chr8 19504047 2 3.28E-06 chr5 168524638 -2 4.56E-06 chr5 64884512 2 4.56E-06 chr4 90582316 -2 7.02E-06 chr4 90582316 -2 7.75E-06 chr4 90582316 -2 7.75E-06 chr3 127558041 2 7.75E-06 chr3 17558041 2 8.10E-06 chr3 1831606 -2 1.06E-05 chr4 4781872 2 8.10E-06 chr4 4781872 2 8.10E-06	rank	CpG Site	chr	position	Sign Consistency	Meta FDR	Meta Beta	Gene	Methylation Status
cg03357456 chr7 102067072 -2 4,53E-07 cg21132297 chr11 43355493 -2 2.24E-06 cg03937517 chr3 133383077 -2 2.76E-06 cg12020733 chr18 68082772 2 2.76E-06 cg01922603 chr8 19504047 2 3.28E-06 cg00809147 chr5 168524638 -2 4.56E-06 cg03409548 chr1 47082691 -2 4.56E-06 cg245156715 chr5 64884512 2 4.56E-06 cg246156715 chr4 47082691 -2 4.56E-06 cg241721910 chr1 172744917 2 4.92E-06 cg217278861 chr3 127558041 2 7.33E-06 cg27278861 chr3 1790434 -2 9.66E-06 cg27278861 chr3 1791715 2 8.09E-06 cg27278861 chr3 1781872 2 1.06E-05 cg0895227 chr1 <td< td=""><td>1</td><td>cg12795959</td><td>chr20</td><td>1569403</td><td>-2</td><td>2.37E-07</td><td>-0.033</td><td>SIRPB1</td><td>hypo</td></td<>	1	cg12795959	chr20	1569403	-2	2.37E-07	-0.033	SIRPB1	hypo
cg21132297 chr11 43355493 -2 2.24E-06 cg03937517 chr13 133383077 -2 2.76E-06 cg12020733 chr18 68082772 2 3.1E-06 cg01922603 chr8 19504047 2 3.28E-06 cg01922603 chr8 19504047 2 3.28E-06 cg00809147 chr5 168524638 -2 4.56E-06 cg03409548 chr1 47082691 -2 4.56E-06 cg26156715 chr5 64884512 2 4.92E-06 cg17721910 chr1 172744917 2 7.02E-06 cg00810717 chr4 90582316 -2 7.33E-06 cg27278861 chr3 127558041 2 7.75E-06 cg27278861 chr3 4781872 2 8.09E-06 cg27278861 chr3 4781872 2 8.09E-06 cg03704653 chr1 4781872 2 1.06E-05 cg0895227 chr1 560430	2	cg03357456	chr7	102067072	-2	4.53E-07	-0.016	PRKRIP1	hypo
cg03937517 chr3 133383077 -2 2.76E-06 cg12020733 chr18 68082772 2 3.1E-06 cg01922603 chr8 19504047 2 3.28E-06 cg00809147 chr5 168524638 -2 4.56E-06 cg03409548 chr1 47082691 -2 4.92E-06 cg26156715 chr5 64884512 2 4.92E-06 cg1721910 chr1 172744917 2 4.92E-06 cg00810717 chr4 90582316 -2 7.02E-06 cg27278861 chr3 127558041 2 7.75E-06 cg22944890 chr2 71901715 2 8.09E-06 cg22944890 chr7 4781872 2 8.10E-06 cg22944890 chr7 4781872 2 8.10E-06 cg03704653 chr1 4781872 2 1.06E-05 cg08952227 chr1 1831606 -2 1.06E-05 cg08952245 chr1 56043017<		cg21132297	chr11	43355493	-2	2.24E-06	-0.025	API5	hypo
cg12020733 chr18 68082772 2 3.11E-06 cg01922603 chr8 19504047 2 3.28E-06 cg00809147 chr5 168524638 -2 4.56E-06 cg03409548 chr1 47082691 -2 4.92E-06 cg26156715 chr5 64884512 2 5.93E-06 cg1721910 chr1 172744917 2 7.02E-06 cg00810717 chr4 90582316 -2 7.75E-06 cg27278861 chr3 127558041 2 7.75E-06 cg22944890 chr2 71901715 2 8.09E-06 cg22944890 chr2 77941872 2 8.10E-06 cg05066096 chr7 4781872 2 8.10E-06 cg03704653 chr1 1831606 -2 1.06E-05 cg08952227 chr1 5604301 -2 1.14E-05 cg089809764 chr1 5604301 -2 1.14E-05 cg256596456 chr1 321825		cg03937517	chr3	133383077	-2	2.76E-06	-0.018	90	hypo
cg01922603 chr8 19504047 2 3.28E-06 cg00809147 chr5 168524638 -2 4.56E-06 cg03409548 chr1 47082691 -2 4.92E-06 cg26156715 chr5 64884512 2 5.93E-06 cg1721910 chr1 172744917 2 7.02E-06 cg00810717 chr4 90582316 -2 7.33E-06 cg27278861 chr3 127558041 2 7.75E-06 cg22944890 chr2 74781872 2 810E-06 cg05066096 chr7 4781872 2 810E-06 cg03704653 chr3 8769344 -2 9.66E-06 cg08952227 chr1 1831606 -2 1.09E-05 cg089809764 chr1 5604301 -2 1.14E-05 cg25596456 chr4 69598331 -2 1.14E-05 cg26596456 chr4 32182518 2 1.33E-05 cg26506456 chr4 49598331<		cg12020733	chr18	68082772	2	3.11E-06	0.020		hyper
cg00809147 chr5 168524638 -2 4.56E-06 cg03409548 chr1 47082691 -2 4.56E-06 cg26156715 chr5 64884512 2 5.93E-06 cg11721910 chr1 172744917 2 7.02E-06 cg00810717 chr4 90582316 -2 7.33E-06 cg27278861 chr3 127558041 2 7.75E-06 cg22944890 chr2 71901715 2 8.09E-06 cg22944890 chr2 4781872 2 8.10E-06 cg05066096 chr7 4781872 2 8.10E-06 cg03704653 chr3 8769344 -2 9.66E-06 cg08952227 chr1 1831606 -2 1.09E-05 cg08952227 chr1 5604301 -2 1.12E-05 cg09809764 chr1 5604301 -2 1.14E-05 cg25656456 chr4 69598331 -2 1.47E-05 cg26506456 chr4 69598331		cg01922603	chr8	19504047	2	3.28E-06	0.035	CSGALNACT1	hyper
cg03409548 chr1 47082691 -2 4,92E-06 cg26156715 chr5 64884512 2 5,93E-06 cg11721910 chr1 172744917 2 7,02E-06 cg00810717 chr4 90582316 -2 7,33E-06 cg27278861 chr3 127558041 2 7,75E-06 cg22944890 chr2 71901715 2 8,09E-06 cg05066096 chr7 4781872 2 8,10E-06 cg03704653 chrX 8769344 -2 9,66E-06 cg08952227 chr1 1831606 -2 1,09E-05 cg08952227 chr1 1831606 -2 1,09E-05 cg08952227 chr1 56043017 -2 1,09E-05 cg0896566 chr1 56043017 -2 1,12E-05 cg2559645 chr1 5698331 -2 1,12E-05 cg2650645 chr1 32182518 2 1,37E-05 cg2660621606 chr1 117746873		cg00809147	chr5	168524638	-2	4.56E-06	-0.033		hypo
cg26156715 chr5 64884512 2 5.93E-06 cg11721910 chr1 172744917 2 7.02E-06 cg00810717 chr4 90582316 -2 7.33E-06 cg27278861 chr3 127558041 2 7.75E-06 cg22944890 chr2 71901715 2 8.09E-06 cg05066096 chr7 4781872 2 8.10E-06 cg03704653 chrX 8769344 -2 9.66E-06 cg08952227 chr16 1831606 -2 1.06E-05 cg08952227 chr16 1831606 -2 1.09E-05 cg09809764 chr17 56043017 -2 1.12E-05 cg25596456 chr4 69598331 -2 1.14E-05 cg26596456 chr4 69598331 -2 1.13E-05 cg26506266 chr4 32182518 2 1.37E-05 cg26609277 chr1 111746873 2 1.47E-05 cg00747162 chr1 3522		cg03409548	chr1	47082691	-2	4.92E-06	-0.032	MOB3C	hypo
cg11721910 chr1 172744917 2 7.02E-06 cg00810717 chr4 90582316 -2 7.33E-06 cg27278861 chr3 127558041 2 7.75E-06 cg22944890 chr2 71901715 2 8.09E-06 cg05066096 chr7 4781872 2 8.10E-06 cg03704653 chrX 8769344 -2 9.66E-06 cg08952227 chr16 1831606 -2 1.06E-05 cg03191369 chr20 22284092 2 1.09E-05 cg09809764 chr17 56043017 -2 1.12E-05 cg25596456 chr4 69598331 -2 1.14E-05 cg2506456 chr4 69598331 -2 1.14E-05 cg26596456 chr4 69598331 -2 1.14E-05 cg2650676 chr4 32182518 2 1.37E-05 cg26609277 chr1 111746873 2 1.47E-05 cg00747162 chr1 35227		cg26156715	chr5	64884512	2	5.93E-06	0.020		hyper
cg00810717 chr4 90582316 -2 7.33E-06 cg27278861 chr3 127558041 2 7.75E-06 cg22944890 chr2 71901715 2 8.09E-06 cg05066096 chr7 4781872 2 8.10E-06 cg03704653 chrX 8769344 -2 9.66E-06 cg08952227 chr16 1831606 -2 1.06E-05 cg03191369 chr20 22284092 2 1.09E-05 cg09809764 chr17 56043017 -2 1.14E-05 cg25596456 chr4 69598331 -2 1.14E-05 cg26596456 chr4 69598331 -2 1.14E-05 cg26506276 chr1 32182518 2 1.33E-05 cg266021606 chr5 82999102 2 1.47E-05 cg00747162 chr1 35227074 -2 1.65E-05 cg23762263 chr2 12908207 -2 1.65E-05		cg11721910	chr1	172744917	2	7.02E-06	0.039	RP1-15D23.2	hyper
cg27278861 chr3 127558041 2 7.75E-06 cg22944890 chr2 71901715 2 8.09E-06 cg05066096 chr7 4781872 2 8.10E-06 cg03704653 chrX 8769344 -2 9.66E-06 cg08952227 chr16 1831606 -2 1.06E-05 cg03191369 chr20 22284092 2 1.09E-05 cg09809764 chr17 56043017 -2 1.14E-05 cg25596456 chr4 69598331 -2 1.14E-05 cg19746753 chr1 32182518 2 1.38E-05 cg260621606 chr3 82999102 2 1.47E-05 cg00621606 chr5 82999102 2 1.47E-05 cg09747162 chr1 35227074 -2 1.65E-05 cg2326263 chr2 12908207 -2 1.65E-05		cg00810717	chr4	90582316	-2	7.33E-06	-0.033	RP11-115D19.1	hypo
cg22944890 chr2 71901715 2 8.09E-06 cg05066096 chr7 4781872 2 8.10E-06 cg03704653 chrX 8769344 -2 9.66E-06 cg0895227 chr16 1831606 -2 1.06E-05 cg03191369 chr20 22284092 2 1.09E-05 cg09809764 chr17 56043017 -2 1.12E-05 cg26596456 chr4 69598331 -2 1.14E-05 cg19746753 chr4 69598331 -2 1.14E-05 cg26609277 chr1 32182518 2 1.33E-05 cg26601606 chr5 82999102 2 1.47E-05 cg06621606 chr5 82999102 2 1.47E-05 cg09747162 chr1 35227074 -2 1.65E-05 cg23261737 chr20 12908207 -2 1.65E-05		cg27278861	chr3	127558041	2	7.75E-06	0.022	MGLL	hyper
cg05066096 chr7 4781872 2 8.10E-06 cg03704653 chrX 8769344 -2 9.66E-06 cg08952227 chr16 1831606 -2 1.06E-05 cg08191369 chr20 22284092 2 1.09E-05 cg09809764 chr17 56043017 -2 1.12E-05 cg26596456 chr4 69598331 -2 1.14E-05 cg19746753 chr1 32182518 2 1.33E-05 cg2609277 chr1 3299102 2 1.47E-05 cg06621606 chr5 82999102 2 1.47E-05 cg09747162 chr1 35227074 -2 1.60E-05 cg23241737 chr20 12908207 -2 1.65E-05 cg23762263 chr2 154730326 -2 1.65E-05		cg22944890	chr2	71901715	2	8.09E-06	0.013	DYSF	hyper
cg03704653 chrX 8769344 -2 9.66E-06 cg0895227 chr16 1831606 -2 1.06E-05 cg03191369 chr20 22284092 2 1.09E-05 cg09809764 chr17 56043017 -2 1.12E-05 cg26596456 chr4 69598331 -2 1.14E-05 cg19746753 chr1 32182518 2 1.33E-05 cg2609277 chr1 111746873 2 1.39E-05 cg06621606 chr5 82999102 2 1.47E-05 cg09747162 chr1 35227074 -2 1.60E-05 cg23241737 chr20 12908207 -2 1.65E-05 cg23762263 chr2 154730326 -2 1.65E-05		cg05066096	chr7	4781872	2	8.10E-06	0.021		hyper
cg08952227 chr16 1831606 -2 1.06E-05 cg03191369 chr20 22284092 2 1.09E-05 cg09809764 chr17 56043017 -2 1.12E-05 cg26596456 chr4 69598331 -2 1.14E-05 cg19746753 chr14 32182518 2 1.33E-05 cg2609277 chr1 111746873 2 1.39E-05 cg06621606 chr5 82999102 2 1.47E-05 cg09747162 chr1 35227074 -2 1.66E-05 cg23241737 chr2 12908207 -2 1.65E-05		cg03704653	chrX	8769344	-2	9.66E-06	-0.024	FAM9A	hypo
cg03191369 chr20 22284092 2 1.09E-05 cg09809764 chr17 56043017 -2 1.12E-05 cg26596456 chr4 69598331 -2 1.14E-05 cg19746753 chr14 32182518 2 1.33E-05 cg22609277 chr1 111746873 2 1.39E-05 cg06621606 chr5 82999102 2 1.47E-05 cg09747162 chr1 35227074 -2 1.66E-05 cg23241737 chr20 12908207 -2 1.65E-05 cg23762263 chr2 154730326 -2 1.65E-05		cg08952227	chr16	1831606	-2	1.06E-05	-0.022	NUBP2	hypo
cg09809764 chr17 56043017 -2 1.12E-05 cg26596456 chr4 69598331 -2 1.14E-05 cg19746753 chr14 32182518 2 1.33E-05 cg22609277 chr1 111746873 2 1.39E-05 cg06621606 chr5 82999102 2 1.47E-05 cg09747162 chr1 35227074 -2 1.60E-05 cg23241737 chr20 12908207 -2 1.65E-05 cg23762263 chr2 154730326 -2 1.65E-05		cg03191369	chr20	22284092	2	1.09E-05	0.012		hyper
cg26596456 chr4 69598331 -2 1.14E-05 cg19746753 chr14 32182518 2 1.33E-05 cg22609277 chr1 111746873 2 1.39E-05 cg06621606 chr5 82999102 2 1.47E-05 cg09747162 chr1 35227074 -2 1.60E-05 cg23241737 chr20 12908207 -2 1.65E-05 cg23762263 chr2 154730326 -2 1.65E-05		cg09809764	chr17	56043017	-2	1.12E-05	-0.022		hypo
cg19746753 chr14 32182518 2 1.33E-05 cg22609277 chr1 111746873 2 1.39E-05 cg06621606 chr5 82999102 2 1.47E-05 cg09747162 chr1 35227074 -2 1.60E-05 cg23241737 chr20 12908207 -2 1.65E-05 cg23762263 chr2 154730326 -2 1.65E-05		cg26596456	chr4	69598331	-2	1.14E-05	-0.018		hypo
cg22609277 chr1 111746873 2 1.39E-05 cg06621606 chr5 82999102 2 1.47E-05 cg09747162 chr1 35227074 -2 1.60E-05 cg23241737 chr20 12908207 -2 1.65E-05 cg23762263 chr2 154730326 -2 1.65E-05		cg19746753	chr14	32182518	2	1.33E-05	0.025	NUBPL	hyper
cg06621606 chr5 82999102 2 1.47E-05 cg09747162 chr1 35227074 -2 1.60E-05 cg23241737 chr20 12908207 -2 1.65E-05 cg23762263 chr2 154730326 -2 1.65E-05		cg22609277	chr1	111746873	2	1.39E-05	0.030	CHI3L2	hyper
cg09747162 chr1 35227074 -2 1.60E-05 cg23241737 chr20 12908207 -2 1.65E-05 cg23762263 chr2 154730326 -2 1.65E-05		cg06621606	chr5	82999102	2	1.47E-05	0.020	ne Ne	hyper
cg23241737 chr20 12908207 -2 1.65E-05 cg23762263 chr2 154730326 -2 1.65E-05		cg09747162	chr1	35227074	-2	1.60E-05	-0.021	RP1-34M23.5	hypo
cg23762263 chr2 154730326 -2 1.65E-05		cg23241737	chr20	12908207	-2	1.65E-05	-0.032	RP5-1069C8.2	hypo
		cg23762263	chr2	154730326	-2	1.65E-05	-0.026	GALNT13	hypo

Methylation Status	hypo	hyper	hypo	hyper	hyper	hypo	hyper	hypo	hyper	hypo	hypo	hypo	hypo	hyper	hypo	hypo	hyper	hypo	hyper	hyper	hyper	hypo	hypo	hyper	hypo
Gene	RNU5F-4P	C8orf80	HADH	TSPAN4		C8orf84		SRSF4	ZBTB20			SNTB1	PDZK11P1	SIM2		FAM71F1	GCNT4	KIAA0284		GLYCTK	C11orf9	CREB3L2	DNAJB4	RP11- 255A11.21	
Meta Beta	-0.022	0.015	-0.025	0.035	0.014	-0.017	0.017	-0.029	0.034	-0.024	-0.015	-0.040	-0.026	0.039	-0.013	-0.015	0.015	-0.020	0.021	0.013	0.018	-0.025	-0.017	0.013	-0.022
Meta FDR	1.79E-05	1.84E-05	1.93E-05	1.95E-05	2.08E-05	2.19E-05	2.33E-05	2.37E-05	2.58E-05	2.73E-05	2.79E-05	2.96E-05	3.04E-05	3.05E-05	3.06E-05	3.14E-05	3.34E-05	3.45E-05	3.50E-05	3.63E-05	3.69E-05	3.74E-05	3.80E-05	4.03E-05	4.04E-05
Sign Consistency	-2	2	-2	2	2	-2	2	-2	2	-2	-2	-2	-2	2	-2	-2	2	-2	2	2	2	-2	-2	2	-2
position	31747831	27936225	108910929	842622	188654304	74031115	30904981	29487000	114328840	81312506	65126816	121718948	47656003	38070639	10666585	128355632	74327277	105332627	57454621	52324261	61541311	137584214	78444087	33602735	14915807
chr	chr12	chr8	chr4	chr11	chr4	chr8	chr6	chr1	chr3	chr8	chr2	chr8	chr1	chr21	chr2	chr7	chr5	chr14	chr12	chr3	chr11	chr7	chr1	chr9	chr5
CpG Site	cg10750929	cg25867383	cg11079189	cg06468208	cg03986546	cg05248004	cg08487909	cg01993027	cg14847818	cg09903756	cg00223042	cg22594690	cg06619077	cg22976224	cg26539736	cg12912245	cg11743470	cg18163342	cg25645008	cg05012617	cg01140770	cg13656809	cg08228724	cg14082582	cg17749710
rank	56	27	28	56	30	31	32	33	34	35	36	37	38	39	40	41	42	43	44	45	46	47	48	49	20

Supplementary Table S2 (partially) - DM CpG that likely affect gene expression. Prioritized DM CpG sites, those that mapped to genes within 200 or 1500 bp of the transcription start site (TSS200, TSS1500), located within the 3' or 5' UTR regions, or CpG sites that were exon bound. This resulted in 2492 CpG-gene pairs

rank	CpG Site	chr	sod	Sign Consistency	Meta FDR	Meta Beta	Gene	Methylation Status
1	cg12795959	chr20	1569403	-2	2.37E-07	-0.03273	SIRPB1	hypo
2	cg03357456	chr7	1.02E+08	-2	4.53E-07	-0.01605	PRKRIP1	hypo
33	cg21132297	chr11	43355493	-2	2.24E-06	-0.02526	API5	hypo
4	cg01922603	chr8	19504047	2	3.28E-06	0.035466	CSGALNACT1	hyper
2	cg03409548	chr1	47082691	-2	4.92E-06	-0.03159	MOB3C	hypo
9	cg27278861	chr3	1.28E+08	2	7.75E-06	0.022348	MGLL	hyper
7	cg22944890	chr2	71901715	2	8.09E-06	0.013318	DYSF	hyper
8	cg03704653	chrX	8769344	-2	9.66E-06	-0.0236	FAM9A	hypo
6	cg08952227	chr16	1831606	-2	1.06E-05	-0.02205	NUBP2	hypo
10	cg19746753	chr14	32182518	2	1.33E-05	0.024665	NUBPL	hyper
11	cg22609277	chr1	1.12E+08	2	1.39E-05	0.029954	CHI3L2	hyper
12	cg23762263	chr2	1.55E+08	-2	1.65E-05	-0.026	GALNT13	hypo
13	cg11079189	chr4	1.09E+08	-2	1.93E-05	-0.02525	HADH	hypo
14	cg06468208	chr11	842622	2	1.95E-05	0.035135	TSPAN4	hyper
15	cg01993027	chr1	29487000	-2	2.37E-05	-0.02929	SRSF4	hypo
16	cg14847818	chr3	1.14E+08	2	2.58E-05	0.034074	ZBTB20	hyper
17	cg22594690	chr8	1.22E+08	-2	2.96E-05	-0.04023	SNTB1	hypo
18	cg06619077	chr1	47656003	-2	3.04E-05	-0.02642	PDZK11P1	hypo
19	cg22976224	chr21	38070639	2	3.05E-05	0.039186	SIM2	hyper
20	cg12912245	chr7	1.28E+08	-2	3.14E-05	-0.0152	FAM71F1	hypo
21	cg11743470	chr5	74327277	2	3.34E-05	0.01451	GCNT4	hyper
22	cg05012617	chr3	52324261	2	3.63E-05	0.012979	GLYCTK	hyper
23	cg13656809	chr7	1.38E+08	-2	3.74E-05	-0.02515	CREB3L2	hypo
24	cg08228724	chr1	78444087	-2	3.80E-05	-0.01701	DNAIB4	hypo

Methylation Status	hyper	hypo	hypo	hypo	hyper	hyper	hyper	hyper	hypo	hypo	hypo	hypo	hyper	hyper	hypo	hyper	hypo	hypo	hypo									
Gene	DLX4	NEFM	BTNL9	AC009264.1	ADAM33	CHURC1- FNTB	ABLIM2	KBTBD6	ZNF485	MOB2	CARS2	ANKRD27	CNKSR3	AIFM1	DAPK3	KIAA1210	PABPC4	CACNA1C	PLEKHF2	PSG9	BMF	NUP93	CCDC138	CRK	OR10J1	BCOR	UGT2B17	EPS8
Meta Beta	0.028347	-0.0203	-0.02569	-0.01882	0.015385	0.01506	0.011709	0.065859	-0.0291	-0.01531	-0.01615	-0.01332	0.013641	-0.02272	-0.02378	0.026506	-0.04079	-0.01659	0.01711	-0.01964	-0.02647	0.041006	0.009591	-0.02335	0.01752	-0.01615	-0.02848	-0.01664
Meta FDR	4.76E-05	4.92E-05	5.07E-05	5.27E-05	5.42E-05	5.60E-05	5.95E-05	6.07E-05	6.35E-05	6.73E-05	6.80E-05	7.82E-05	8.05E-05	8.42E-05	8.59E-05	8.66E-05	8.99E-05	9.35E-05	9.50E-05	9.68E-05	9.75E-05	9.76E-05	9.91E-05	0.000106	0.000107	0.0001111	0.000116	0.000116
Sign Consistency	2	-2	-2	-2	2	2	2	2	-2	-2	-2	-2	2	-2	-2	2	-2	-2	2	-2	-2	2	2	-2	2	-2	-2	-2
sod	48046859	24770189	1.8E+08	1.37E+08	3650493	65383590	8149665	41707137	44100669	1492667	1.11E+08	33162885	1.55E+08	1.29E+08	3969950	1.18E+08	40026520	2645161	96144768	43774776	40399131	56817380	1.09E+08	1359781	1.59E+08	40037471	69433682	15924004
chr	chr17	chr8	chr5	chr7	chr20	chr14	chr4	chr13	chr10	chr11	chr13	chr19	chr6	chrX	chr19	chrX	chr1	chr12	chr8	chr19	chr15	chr16	chr2	chr17	chr1	chrX	chr4	chr12
CpG Site	cg13206920	cg26174464	cg04903465	cg27342559	cg17401106	cg01932468	cg19222680	cg14792031	86606660go	cg05806529	cg25756044	cg01442620	cg20919556	cg11593337	cg13144588	cg06761424	cg11742479	cg09650018	cg05189165	cg23749091	cg08131309	cg11164293	cg00607919	cg06972217	cg24994494	cg11844737	cg19481811	cg12440131
rank	25	26	27	28	29	30	31	32	33	34	35	36	37	38	39	40	41	42	43	44	45	46	47	48	49	20	51	52

Supplementary Table S4 (partially) - GO Pathway Enrichment analysis of ML-tCpGs

Enrichmont Torm		IICOIIIIIOII	Enrichment	
	Bonferroni	Genes	Ratio	overlapGenes
regulation of coagulation	3.58E-04	6	13.46	ABAT ANXA5 CAV1 EPHB2 F3 SERPINE2 PLAT THBD ADTRP
regulation of blood coagulation	3.44E-03	8	12.78	ABAT CAV1 EPHB2 F3 SERPINE2 PLAT THBD ADTRP
regulation of hemostasis	4.49E-03	8	12.36	ABAT CAV1 EPHB2 F3 SERPINE2 PLAT THBD ADTRP
wound healing	5.85E-03	17	4.40	ABAT ANXA5 CAV1 CD44 EPHB2 F3 HSPB1 ITGA5 SERPINE2 PLAT PPARD THBD VAV2 TFPI2 EPB41L4B FERMT1 ADTRP
blood coagulation	9.23E-03	12	6.25	ABAT ANXA5 CAV1 EPHB2 F3 HSPB1 SERPINE2 PLAT THBD VAV2 TFPI2 ADTRP
coagulation	1.04E-02	12	6.18	ABAT ANXA5 CAV1 EPHB2 F3 HSPB1 SERPINE2 PLAT THBD VAV2 TFPI2 ADTRP
hemostasis	1.24E-02	12	80.9	ABAT ANXA5 CAV1 EPHB2 F3 HSPB1 SERPINE2 PLAT THBD VAV2 TFPI2 ADTRP
anatomical structure morphogenesis	1.27E-02	50	1.97	FMNL1 CAV1 CD44 CDH18 CYP1B1 DLX1 DUSP1 DUSP5 EPHB2 F3 FLII KATZA HSPB1 I L4R IL.7R ITGA5 LAMC2 STMN1 MAPT MET NBL1 NCAM1 SERPINE2 PTGIS CXCL12 SG K1 SYT1 VAV2 WNT9A HMGA2 FIG4 FGFBP1 RAPGEF3 LYVE1 PACSIN2 RUFY3 CRB1 C DH20 SH3KBP1 CHST11 IRX4 ANGPTL4 GCNT4 FERMT1 CSRNP1 CRISPLD1 CRISPLD2 ADTRP TMEM182 FREM2
regulation of body fluid levels	1.94E-02	15	4.56	ABAT ANXA5 CAV1 EPHB2 F3 HSPB1 STMN1 MET SERPINE2 PLAT THBD VAV2 TFPI2 ALOXE3 ADTRP
caveola assembly	2.15E-02	33	94.23	CAV1 CAV2 PACSIN2
negative regulation of response to stimulus	2.55E-02	35	2.33	ABAT CAV1 CAV2 CD44 CSK DLX1 DUSP1 DUSP5 EPHB2 HIC1 HSPA1B HSPB1 IL4R IL7 R STMN1 MET NBL1 SERPINE2 PLAT PPARD PTGIS PTPRE CXCL12 THBD HMGA2 GPR C5A HOMER3 SLC27A4 SH3BP4 SAMHD1 CHST11 FERMT1 ADTRP STYXL2 MRAP2